

Finite-volume effects in the Polyakov-loop extended Nambu-Jona-Lasinio model with a chiral chemical potential

Zan Pan^{1,2}, Zhu-Fang Cui³, Chao-Hsi Chang^{1,2,4,*} and Hong-Shi Zong^{1,3,5†}

¹Key Laboratory of Theoretical Physics, Institute of Theoretical Physics, CAS, Beijing, 100190, China

²School of Physical Sciences, University of Chinese Academy of Sciences, Beijing 100049, China

³Department of Physics, Nanjing University, Nanjing 210093, China

⁴CCAST (World Laboratory), P.O. Box 8730, Beijing 100190, China and

⁵Joint Center for Particle, Nuclear Physics and Cosmology, Nanjing 210093, China

(Dated: May 3, 2016)

We investigate the impact of finite-volume effects on the chiral symmetry restoration and the deconfinement transition of the phase diagram of quantum chromodynamics, using the Polyakov-loop extended Nambu-Jona-Lasinio model for $N_f = 2$ quark flavors in presence of a chiral chemical potential μ_5 . Numerical results verify that the chiral chemical potential does not change the critical exponents but significantly shifts the location of critical end point. The ratios μ_c/μ_{5c} and T_c/T_{5c} are significantly affected by the system sizes R . When R is large, T_c increases slowly with μ_5 ; when R is small, T_c decreases first and then increases with μ_5 . For a fixed μ_5 , we can also determine a R_{\min} such that the critical end point vanishes when $R < R_{\min}$, and the whole phase diagram becomes a crossover, which can provide some hints to the heavy-ion collision experiments aiming at the search of the possible critical end point.

PACS numbers: 12.38.Aw, 12.38.Mh, 12.39.-x, 25.75.Nq

I. INTRODUCTION

The thermodynamics of strongly interacting matter under extreme conditions of temperature and density is a profound and challenging area of overlap between statistical, particle and nuclear physics. A deep understanding of its phase structure is expected to bring some insights on many fundamental problems such as hadron structure, compact stars, and the early universe [1, 2]. Experiments with heavy-ion collisions such as the BNL Relativistic Heavy-Ion Collider (RHIC) and the CERN Large Hadron Collider (LHC) are continuing active investigations on the strongly interacting matter in the laboratory [3, 4].

It is expected that quantum chromodynamics (QCD) could lead to a rich phase structure [5]. Lattice simulations from the first principle have revealed that confined quarks will become released to quark-gluon plasma around the temperature $T_c = 154(9)$ MeV [6, 7]. However, due to the sign problem, Monte Carlo methods can only be applied to the states around zero baryon density. Therefore, effective models which exhibit the features of color confinement and spontaneous chiral symmetry breaking are more feasible to be used to study the phase structure of QCD. Here, we will adopt the Polyakov-loop extended Nambu-Jona-Lasinio (PNJL) model [8–11].

In the PNJL model, it is found that the chiral symmetry restoration and deconfinement transition may coincide and they are of the first order [10]. Discontinuities appear simultaneously in their order parameters, that is the chiral condensate σ and the Polyakov loop L . A nontrivial critical end point (CEP) also exists at finite

temperature T and quark chemical potential μ , which indicates a coincidence of second-order phase transitions. To characterize the chirality imbalance $N_5 = N_R - N_L$ of strongly interacting matter, the chiral (or axial) chemical potential μ_5 is introduced to mimic the effect of the topological charge changing transitions that are naturally expected by the QCD anomaly relation [12]. This also leads to a novel idea proposed in [13] to detect the CEP by simulating QCD with μ_5 : CEP can be continued to a critical end point at the μ_5 - T plane denoted by CEP₅, which is accessible to lattice QCD simulations of grand-canonical ensembles. If lattice simulations find CEP₅, this should be seen as a signal of the existence of the CEP in QCD. As we know, physical systems in the same universality class all share the same critical exponents. To check the reasonableness of this continuation, we would like to know what are the impacts on the critical exponents brought by the introducing of a μ_5 .

For the two-flavor PNJL model, there are unphysical decays of hadrons to quarks due to the spurious poles in the quark loop diagrams [14, 15]. Introducing a lower momentum cutoff to mimic confining effects of strong interaction helps to address this problem. This is the starting point of how we incorporate the finite-volume effects. In experiments with heavy-ion collisions, the strongly interacting matter formed through the energy deposition of the colliding particle obviously has a finite volume. Therefore, it is very important to have a clear understanding of the finite-volume effects to fully contemplate the thermodynamic phases. In the context of heavy-ion collisions, the importance of finite-volume effects in the thermodynamics of strong interaction may be brought forward with the help of finite size scaling analysis [16, 17]. In the past years, many theoretical studies of finite-volume effects have been performed on NJL mod-

* Email: zhangzx@itp.ac.cn

† Email: zonghs@nju.edu.cn

els [18–20]. However, only recently the studies on the thermodynamic properties of strongly interacting matter in a finite volume using the PNJL models have aroused increasing attention [21–23].

Our paper is organized as follows. First, in Sec. II we briefly review the PNJL model with a chiral chemical potential in the mean field approximation. In Sec. III, numerical results on chiral symmetry restoration and deconfinement transition are presented for $N_f = 2$ with the infinite size. We also verify that the chiral chemical potential does not impact on the value of critical exponents. By introducing the lower momentum cutoff, we investigate its finite-volume effects in Sec. IV. Finally, in Sec. V we summarize our results and make some conclusions.

II. THE POLYAKOV-LOOP EXTENDED NAMBU-JONA-LASINIO MODEL

In this section, we review the PNJL model in the mean field approximation [9, 11]. The Lagrangian is given by

$$\mathcal{L} = \bar{\psi}(i\not{D} - m)\psi + G [(\bar{\psi}\psi)^2 + (i\bar{\psi}\gamma_5\boldsymbol{\tau}\psi)^2] - \mathcal{U}(L, L^\dagger, T), \quad (1)$$

where $\psi = (u, d)$ represents the quark fields; the number of flavors is taken as $N_f = 2$, and the number of colors is $N_c = 3$; the two-flavor current quark mass matrix is $m = \text{diag}(m_u, m_d)$, and we shall work in the isospin-symmetric limit with $m_u = m_d$; $\boldsymbol{\tau}$ corresponds to the Pauli matrices in flavor space.

The potential term $\mathcal{U}(L, L^\dagger, T)$ is the effective potential expressed in terms of the traced Polyakov loop L and its conjugate

$$L = \frac{1}{N_c} \text{Tr}_c W, \quad L^\dagger = \frac{1}{N_c} \text{Tr}_c W^\dagger. \quad (2)$$

The Polyakov loop W is a matrix in color space explicitly given by

$$W = \mathcal{P} \exp \left[i \int_0^\beta A_4(\mathbf{x}, \tau) d\tau \right], \quad (3)$$

where $\beta = 1/T$ is the inverse temperature and $A_4 = iA^0$. In the Polyakov gauge, W can have a diagonal representation in color space [8]. The traced Polyakov loop L is an exact order parameter of spontaneous \mathbb{Z}_3 symmetry breaking in pure gauge theory. Although in full QCD the presence of dynamical quarks explicitly breaks the \mathbb{Z}_3 symmetry, it still seems to be a good indicator of the deconfinement phase transition. To incorporate the confinement or deconfinement properties, we have introduced a Polyakov-loop-dependent coupling constant G as

$$G = g[1 - \alpha_1 LL^\dagger - \alpha_2(L^3 + L^{\dagger 3})]. \quad (4)$$

For simplicity we will take $L = L^\dagger$. The numerical values of α_1 and α_2 can be obtained by a best fit of lattice data at zero and imaginary chemical potential, which leads to $\alpha_1 = \alpha_2 = 0.2$.

In the PNJL model, the simplest way to treat quark matter with chirality imbalance $N_5 = N_R - N_L$ is to introduce a chiral chemical potential μ_5 conjugated to chiral density n_5 [13, 24, 25]. At the Lagrangian level, this amounts to adding the chiral density operator $\mu_5 \bar{\psi} \gamma^0 \gamma^5 \psi$ to Eq. (1). This procedure is similar to how we study systems at finite quark number by adding a quark chemical potential μ that induces a net quark density n .

Making the mean field approximation and performing the path integral over the quark field, we can obtain the thermodynamic potential density \mathcal{V} at the one-loop level

$$\begin{aligned} \mathcal{V} = & \mathcal{U}(L, L^\dagger, T) + G\sigma^2 - N_c N_f \sum_{s=\pm 1} \int \frac{d^3\mathbf{p}}{(2\pi)^3} \omega_s \\ & - N_f \sum_{s=\pm 1} \int \frac{d^3\mathbf{p}}{(2\pi)^3} T \log(F_+ F_-), \end{aligned} \quad (5)$$

where $\sigma = \langle \bar{\psi} \psi \rangle$ is the chiral condensate and relates to the effective quark mass M as

$$M = m - 2G\sigma. \quad (6)$$

The index s denotes the helicity projection and

$$\omega_s = \sqrt{(|\mathbf{p}|s - \mu_5)^2 + M^2} \quad (7)$$

is the pole of the quark propagator. The momentum integral of ω_s corresponds to the vacuum quark fluctuations. It is divergent and can be regularized by introducing the momentum cutoff Λ .

The last term in Eq. (5) is responsible for the statistical properties of the model at low temperature. Therein we have introduced the functions

$$\begin{aligned} F_- &= 1 + 3Le^{-\beta(\omega_s - \mu)} + 3L^\dagger e^{-2\beta(\omega_s - \mu)} + e^{-3\beta(\omega_s - \mu)}, \\ F_+ &= 1 + 3L^\dagger e^{-\beta(\omega_s + \mu)} + 3Le^{-2\beta(\omega_s + \mu)} + e^{-3\beta(\omega_s + \mu)}. \end{aligned} \quad (8)$$

In order to reproduce the pure gluonic lattice data with $N_c = 3$, the potential term \mathcal{U} is taken as the following form

$$\begin{aligned} \mathcal{U}(L, L^\dagger, T) = & T^4 \left\{ -\frac{1}{2} a(T) LL^\dagger + b(T) \ln [1 - 6LL^\dagger \right. \\ & \left. + 4(L^3 + L^{\dagger 3}) - 3(LL^\dagger)^2] \right\}, \end{aligned} \quad (9)$$

where the model parameters are given by

$$a(T) = a_0 + a_1 \left(\frac{T_0}{T} \right) + a_2 \left(\frac{T_0}{T} \right)^2, \quad (10)$$

$$b(T) = b_3 \left(\frac{T_0}{T} \right)^3. \quad (11)$$

The choice of coefficients reads

$$a_0 = 3.51, \quad a_1 = -2.47, \quad a_2 = 15.2, \quad b_3 = -1.75. \quad (12)$$

Other numerical parameters used in our calculation are also taken as the same as those in [11]

$$\begin{aligned} T_0 &= 190 \text{ MeV}, & \Lambda &= 631.5 \text{ MeV}, \\ m &= 5.5 \text{ MeV}, & g &= 5.498 \times 10^{-6} \text{ MeV}^{-2}. \end{aligned} \quad (13)$$

III. CHIRAL SYMMETRY RESTORATION AND DECONFINEMENT TRANSITION

For any given (μ, μ_5, T) , we can obtain the corresponding value of σ and L by solving the gap equations

$$\frac{\partial \mathcal{V}}{\partial \sigma} = 0, \quad \frac{\partial \mathcal{V}}{\partial L} = 0. \quad (14)$$

However, this approach is hard to work in practice due to the difficulty in solving the coupled integral equations by means of iterative methods. Moreover, the solutions of these equations do not necessarily yield a global minimum. There are possibilities that they may yield a local minimum or even a maximum. We need check that the solutions yield a global minimum when they are inserted back into (5). For a better approach, we can solve the problem in the other way: solving Eqs. (14) is equivalent to find the minima of the potential function \mathcal{V} . This reduces to the famous problem of multidimensional minimization, where we can use the efficient Nelder-Mead simplex algorithm.

First, we consider the case of $\mu_5 = 0$. As can be seen from Fig. 1, the discontinuity of the effective mass M and the Polyakov loop L vanishes simultaneously at the same point, which determines the CEP as $(\mu_c, T_c) = (172.7, 159.2)$. Our calculation of the critical temperature is in good agreement with the result $T_c = 154(9)$ MeV from lattice QCD [6]. Although there is a long-standing debate on whether the chiral symmetry restoration and deconfinement transition have an one-to-one correspondence or not [26], they coincide exactly in our PNJL model and are both of first-order transitions.

For $\mu = 0$, we can also determine the location of CEP₅ as $(\mu_{5c}, T_{5c}) = (307.6, 166.1)$, which is plotted in Fig. 2. It is interesting that the critical temperature is almost unchanged in the continuation of CP to CEP₅. In [13], a novel idea to locate the CEP has been suggested by using the relations μ_c/μ_{5c} . If lattice simulations find CEP₅, this should be seen as a signal of the existence of the CEP in QCD.

As the linear response of the physical system to some external field, susceptibilities are widely used to study the phase transitions of strongly interacting matter [27]. Here, we mainly discuss three kinds of susceptibilities: the vector susceptibility χ_v , the axial-vector susceptibility χ_{av} , and the thermal susceptibility χ_T . They are defined as follows

$$\chi_v = \frac{\partial \sigma}{\partial \mu}, \quad \chi_{av} = \frac{\partial \sigma}{\partial \mu_5}, \quad \chi_T = \frac{\partial \sigma}{\partial T}. \quad (15)$$

All these susceptibilities are singular at the CEP or CEP₅ and are continuous in the crossover region. We can also

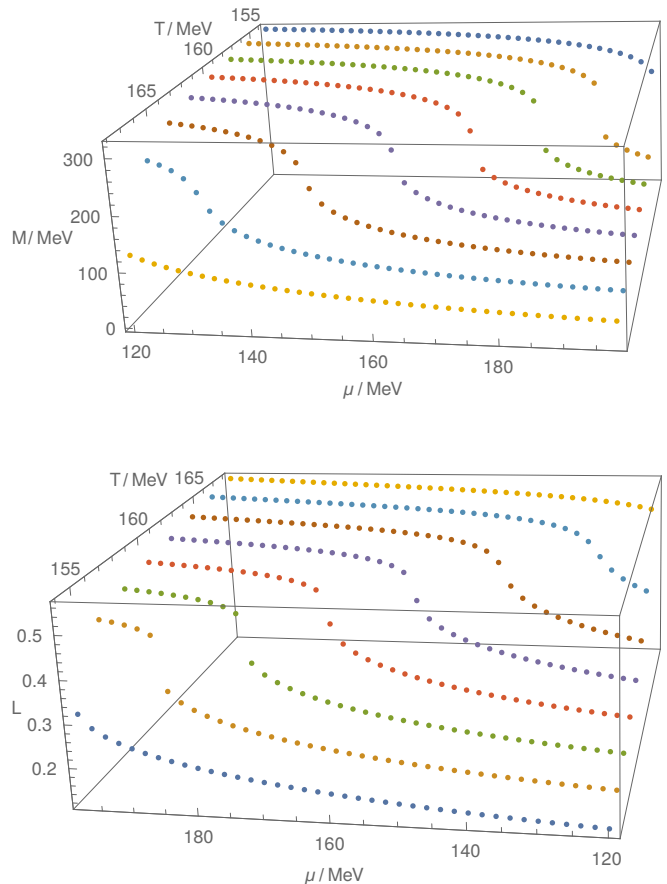


FIG. 1. (color online). 3D plot for the effective mass M (upper panel) in the μ - T - M space and the Polyakov loop L (lower panel) in the μ - T - L space near the CEP $(\mu_c, T_c) = (172.7, 159.2)$, where $\mu_5 = 0$.

use this fact to accurately identify the location of CEP or CEP₅.

As we know, a susceptibility in the vicinity of CEP or CEP₅ diverges in the power law with the so-called critical exponent γ . These exponents are only dependent on the dimension of space and the order parameter and do not involve the details of microscopic dynamics. Different systems in the same universality class all share the same critical behavior. For simplicity, we can choose to calculate the critical exponents in a specific direction denoted by \rightarrow : the path from lower μ or μ_5 toward higher μ_c or μ_{5c} with the temperature fixed $T = T_c$. Using the linear logarithm fit, we obtain

$$\log \chi = -\gamma \log |T - T_c| + \text{const}. \quad (16)$$

The critical exponent of the vector-scalar susceptibility in the direction \rightarrow is calculated in Fig. 3.

Similarly, we mark the other directions as \leftarrow , \uparrow , \downarrow for the path from higher μ or μ_5 toward μ_c or μ_{5c} , the path from lower T toward T_c , and the path from higher T

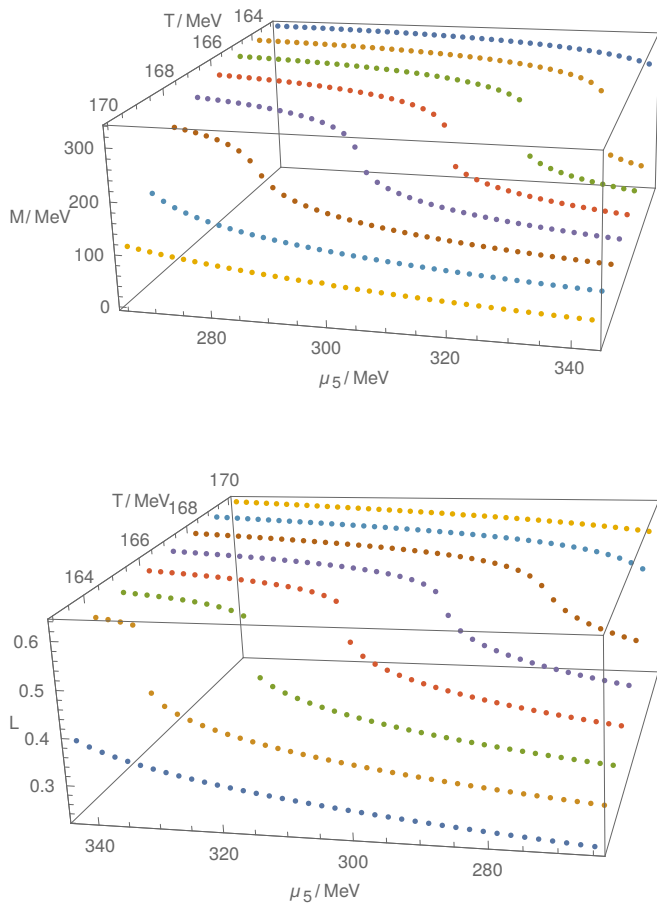


FIG. 2. (color online). 3D plot for the effective mass M (upper panel) in the μ_5 - T - M space and the Polyakov loop L (lower panel) in the μ_5 - T - L space near the CEP₅ (μ_{5c}, T_{5c}) = (307.6, 166.1), where $\mu = 0$.

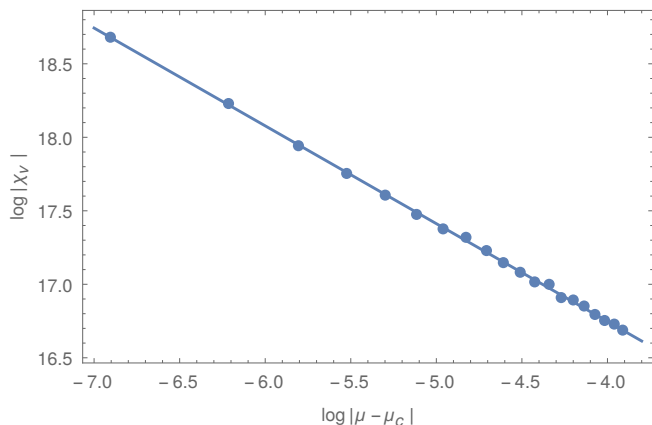


FIG. 3. Linear fit of the logarithm of the vector-scalar susceptibility χ_v as a function of $\log|\mu - \mu_c|$ at the fixed temperature T_c in the direction \rightarrow , where $\mu_5 = 0$. The critical exponent γ_v is calculated from the slope as 0.665 ± 0.030 .

toward T_c respectively. In Table I, we calculate the critical exponents of χ_v and χ_T in these four directions for $\mu_5 = 0$; in Table II, we calculate the critical exponents of χ_{av} and χ_T for $\mu = 0$. They all agree with the mean field predictions about the universality [28, 29]. In [30], more critical exponents are calculated for the NJL model.

As what the Svetitsky-Yaffe conjecture states [31], the critical behavior of a pure SU(3) gauge theory at deconfinement is in the same universality class as the order-disorder transition in the corresponding \mathbb{Z}_3 spin theory (the so-called three-state Potts model) of the same spatial dimension. Whereas the Pisarski-Wilczek conjecture predicts the chiral symmetry restoration in QCD with two species of massless quarks to be in the universality class of an O(4) symmetric spin model [32]. However, in our PNJL model these two transitions coincide exactly and thus have the same exponents.

For $\mu_5 \neq 0$ and $\mu \neq 0$, CEP will naturally evolve into CEP₅. The discontinuity of the effective mass and the Polyakov loop always vanishes at the same CEP, and the chiral symmetry restoration and the deconfinement transition coincide exactly. The projection of the evolution of CEP on the μ - μ_5 plane is illustrated in Fig. 4, which is also in good agreement with the results in [13]. Furthermore, we verify that the nonzero chiral chemical potential does not change the critical exponents, and that γ_v , γ_{av} and γ_T are all approximately equal to $2/3$. This implies that our continuation of the CEP of the QCD phase diagram to a fictitious CEP belonging to a phase diagram in the μ_5 - T plane is reasonable.

TABLE I. Critical exponents for $\mu_5 = 0$, where the CEP is calculated as $(\mu_c, T_c) = (172.7, 159.2)$.

Critical exponent	Path	Numerical result	MF exponent
γ_v	\rightarrow	0.665 ± 0.030	
	\leftarrow	0.636 ± 0.059	$\frac{2}{3}$
	\uparrow	0.679 ± 0.061	$\frac{2}{3}$
	\downarrow	0.659 ± 0.085	
γ_T	\rightarrow	0.658 ± 0.014	
	\leftarrow	0.664 ± 0.010	$\frac{2}{3}$
	\uparrow	0.671 ± 0.012	$\frac{2}{3}$
	\downarrow	0.664 ± 0.017	

IV. FINITE-VOLUME EFFECTS

Since the strongly interacting matter formed through the energy deposition of colliding particles obviously has a finite volume, it is very important to have a clear understanding of the finite-volume effects to fully contemplate the thermodynamic phases that may be created in the experiments. In Refs. [23, 33], the variations of susceptibilities with temperature for different system sizes have

TABLE II. Critical exponents for $\mu = 0$, where the CEP_5 is calculated as $(\mu_{5c}, T_{5c}) = (307.6, 166.1)$.

Critical exponent	Path	Numerical result	MF exponent
γ_{av}	\rightarrow	0.697 ± 0.068	
	\leftarrow	0.717 ± 0.082	$\frac{2}{3}$
	\uparrow	0.694 ± 0.155	$\frac{2}{3}$
	\downarrow	0.690 ± 0.172	
γ_T	\rightarrow	0.668 ± 0.042	
	\leftarrow	0.728 ± 0.061	$\frac{2}{3}$
	\uparrow	0.684 ± 0.013	$\frac{2}{3}$
	\downarrow	0.671 ± 0.016	

been discussed. In this section, we only focus on the finite-volume effects regarding the CEP and CEP_5 .

To incorporate the finite-volume effects, we use a lower momentum cutoff $\lambda = \pi/R$, where R is the system size of a cubic volume $V = R^3$. Then we rewrite the thermodynamic potential density (5) as

$$\begin{aligned} \mathcal{V} = & \mathcal{U}(L, L^\dagger, T) + G\sigma^2 - N_c N_f \sum_{s=\pm 1} \int_{\lambda}^{\Lambda} \frac{d^3\mathbf{p}}{(2\pi)^3} \omega_s \\ & - N_f \sum_{s=\pm 1} \int_{\lambda}^{\infty} \frac{d^3\mathbf{p}}{(2\pi)^3} T \log(F_+ F_-). \end{aligned} \quad (17)$$

Here, we have taken up several simplifications. The infinite sum is considered as an integration over a continuous variation of momentum with the lower cutoff. We also neglect the surface and curvature effects, and do not modify any other mean field parameters of the PNJL model. The same way in discussing finite-volume effects can be found in [22, 23]. Other methods include the Monte Carlo simulation [21] and the renormalization group approach [34]. When $\lambda = 0$, Eq. (17) reduces to the case of the infinite volume corresponding to $R = \infty$.

Following the same procedure in the previous section, we can locate the CEP or CEP_5 and calculate the critical exponents for different system sizes. It has been verified that the system size R does not affect the critical exponents. In Fig. 4, we plot the projection of the evolution of CEP to CEP_5 on the μ - μ_5 plane for different system sizes: $R = \infty, 4 \text{ fm}$, and 3 fm . As can be seen clearly, the finite-volume effects become more and more manifest as R decreases and are more important for lower μ_5 . We also found that the CEP vanishes at a R_{\min} , whose value is estimated to be 2.1 fm . When $R < R_{\min}$, the whole phase diagram becomes a crossover. Our numerical results in Table III also show that the ratios μ_c/μ_{5c} and T_c/T_{5c} are significantly affected by different system sizes. If we use the idea proposed in [13] to locate CEP, the finite-volume effects on these ratios should be considered.

In Fig. 5, we plot the projection of the evolution of CEP on the μ_5 - T plane for different system sizes. We

can see that the relations between T_c and μ_5 are intriguing: when R is large, T_c increases slowly with μ_5 ; when R is small, T_c decreases first and then increases with μ_5 . For large volumes, our results are qualitatively consistent with the results obtained within the framework of Dyson-Schwinger equations [35] and the lattice simulation [36]. However, we should point out that other studies using different models or methods [24, 25, 37, 38] have given opposite results: T_c decreases with μ_5 . In our calculations, the dependence of T_c on μ_5 has been significantly changed by the system sizes, which can be seen as an indicator of the importance of studies on finite-volume effects in effective models.

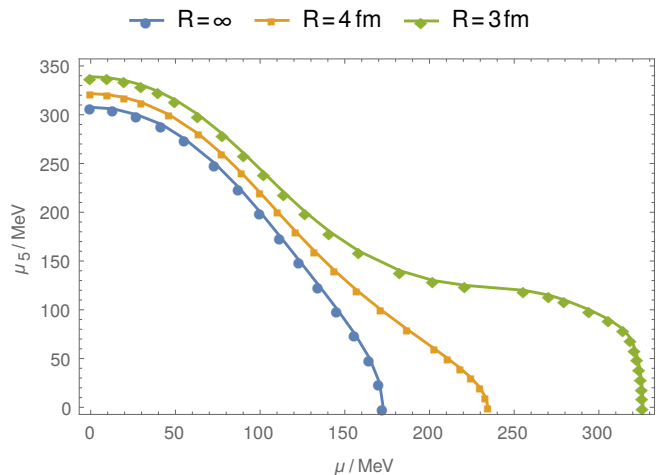


FIG. 4. (color online). Projection of the evolution of CEP on the μ - μ_5 plane for different system sizes: $R = \infty, 4 \text{ fm}$, and 3 fm .

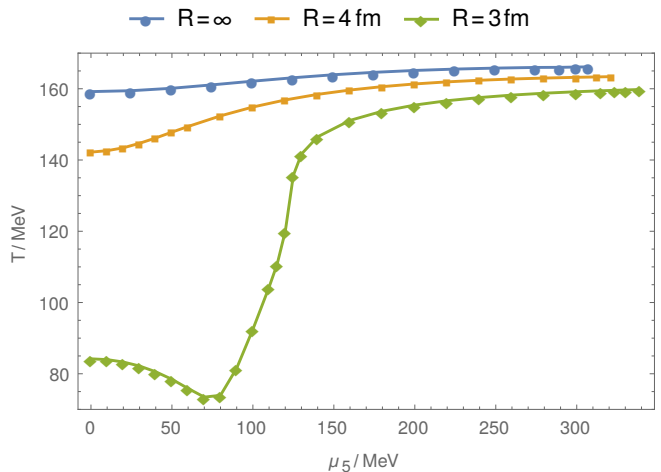


FIG. 5. (color online). Projection of the evolution of CEP on the μ_5 - T plane for different system sizes: $R = \infty, 4 \text{ fm}$, and 3 fm .

Another point of interest is to study the shift of CEP with respect to the system size on the phase diagram. In

TABLE III. Numerical relations between CEP and CEP₅ for different system sizes.

R	(μ_c, T_c)	(μ_{5c}, T_{5c})	$(\mu_c/\mu_{5c}, T_c/T_{5c})$
∞	(172.7, 159.2)	(307.6, 166.1)	(0.561, 0.958)
5 fm	(194.5, 153.6)	(314.9, 164.7)	(0.618, 0.933)
4 fm	(234.6, 142.2)	(321.6, 163.4)	(0.729, 0.870)
3 fm	(326.0, 84.2)	(339.0, 159.8)	(0.962, 0.527)

Fig. 6, we plot the projection of the evolution of CEP on the μ - T plane for fixed chiral chemical potential: $\mu_5 = 0$, 100 MeV, and 200 MeV, varying in the system sizes from $R = \infty$ with the highest critical temperature to R_{\min} with the lowest critical temperature. The corresponding values of R_{\min} are estimated around 2.1 fm, 2.0 fm, and 1.6 fm respectively. It is interesting to note that the relation between critical temperature and the system size may be nonmonotonic for some values of the chiral chemical potential such as $\mu_5 = 200$ MeV.

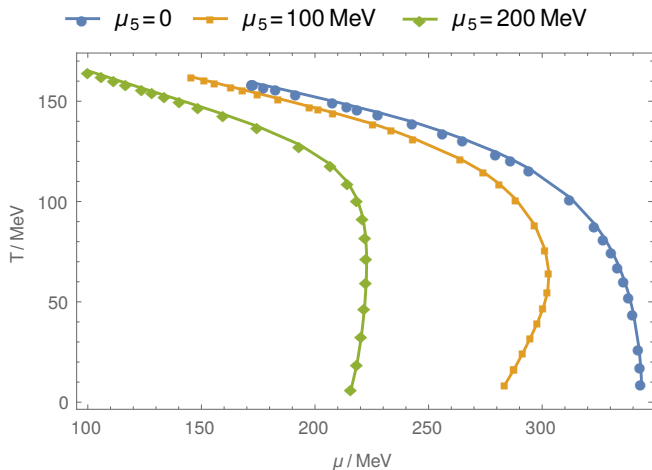


FIG. 6. (color online). Projection of the evolution of CEP on the μ - T plane for fixed chiral chemical potential: $\mu_5 = 0$, 100 MeV, and 200 MeV, varying in the system sizes from $R = \infty$ with the highest critical temperature to R_{\min} with the lowest critical temperature. The corresponding values of R_{\min} are estimated around 2.1 fm, 2.0 fm, and 1.6 fm respectively.

Our results on the finite-volume effects may have significant implications for heavy-ion collision experiments. As we know, these effects depend on the size of the colliding nuclei, the center of mass energy \sqrt{s} , and the centrality of collisions. In our PNJL model, \sqrt{s} relates to the temperature T and the centrality of collisions is characterized by the chiral chemical potential μ_5 . It is expected that our results can provide some hints to the experiments aiming at the search of the possible criti-

cal end point. Although there have been many efforts to estimate the system size [39–42], no general consensus have been reached. In [43], the system volume for Pb-Pb collisions with \sqrt{s} in the range of 62.4 to 2760 GeV has been estimated to vary from 50 to 250 fm³, corresponding to a system size from 3 to 6 fm. Given that these are the volumes at the time of freeze out, one may expect an even smaller system size at the initial equilibration time [41, 42]. Since the PNJL model also adopts several approximations, there may exist some uncertainties on our numerical results.

V. SUMMARY AND CONCLUSION

To summarize, we have discussed the chiral symmetry restoration and the deconfinement transition of the phase diagram of QCD using the PNJL model. To consider the impacts of chirality imbalance $N_5 = N_R - N_L$, a chiral chemical potential μ_5 is introduced. The discontinuity of the effective mass and the Polyakov loop always vanishes at the same CEP, and the two transitions coincide exactly. Three kinds of susceptibilities are defined and the corresponding critical exponents are calculated. All the critical exponents are approximately equal to 2/3. We also verify that the chiral chemical potential does not change the critical exponents. This implies that our continuation of the CEP of the QCD phase diagram to a fictitious CEP belonging to a phase diagram in the μ_5 - T plane is reasonable.

By introducing a lower momentum cutoff in the integration, we investigate the finite-volume effects in our PNJL model. The finite-volume effects become more and more manifest as R decreases and are more important for lower μ_5 . Numerical results show that the ratios μ_c/μ_{5c} and T_c/T_{5c} are significantly affected by the system sizes R . When R is large, T_c increases slowly with μ_5 ; when R is small, T_c decreases first and then increases with μ_5 . For a fixed μ_5 , we can also determine a R_{\min} such that the CEP vanishes when $R < R_{\min}$, and the whole phase diagram becomes a crossover. The corresponding values of R_{\min} for $\mu_5 = 0$, 100 MeV, and 200 MeV are estimated around 2.1 fm, 2.0 fm, and 1.6 fm respectively.

ACKNOWLEDGMENTS

This work is supported in part by the National Natural Science Foundation of China (under the Grants No. 11147001, No. 11275097, No. 11275243, No. 11475085, and No. 11535005), the China Postdoctoral Science Foundation (under the Grant No. 2015M581765), and the Jiangsu Planned Projects for Postdoctoral Research Funds (under the Grant No. 1402006C).

-
- [1] K. Rajagopal and F. Wilczek, in *At the Frontier of Particle Physics: Handbook of QCD*, Vol. 3, edited by M. Shifman (World Scientific, 2001) pp. 2061–2151.
- [2] H. Satz, *Extreme States of Matter in Strong Interaction Physics*, Lecture Notes in Physics, Vol. 841 (Springer Berlin Heidelberg, 2012).
- [3] L. Adamczyk *et al.* (STAR Collaboration), *Phys. Rev. Lett.* **112**, 032302 (2014).
- [4] B. Abelev *et al.*, *Phys. Lett. B* **739**, 139 (2014).
- [5] K. Fukushima and T. Hatsuda, *Rep. Prog. Phys.* **74**, 014001 (2011).
- [6] A. Bazavov *et al.* (HotQCD Collaboration), *Phys. Rev. D* **85**, 054503 (2012).
- [7] P. Petreczky, *J. Phys. G* **39**, 093002 (2012).
- [8] K. Fukushima, *Phys. Lett. B* **591**, 277 (2004).
- [9] C. Ratti, M. A. Thaler, and W. Weise, *Phys. Rev. D* **73**, 014019 (2006).
- [10] Y. Sakai, T. Sasaki, H. Kouno, and M. Yahiro, *Phys. Rev. D* **82**, 076003 (2010).
- [11] R. Gatto and M. Ruggieri, *Phys. Rev. D* **85**, 054013 (2012).
- [12] K. Fukushima, D. E. Kharzeev, and H. J. Warringa, *Phys. Rev. D* **78**, 074033 (2008).
- [13] M. Ruggieri, *Phys. Rev. D* **84**, 014011 (2011).
- [14] H. Hansen, W. M. Alberico, A. Beraudo, A. Molinari, M. Nardi, and C. Ratti, *Phys. Rev. D* **75**, 065004 (2007).
- [15] D. Blaschke, A. Dubinin, and M. Buballa, *Phys. Rev. D* **91**, 125040 (2015).
- [16] L. F. Palhares, E. S. Fraga, and T. Kodama, *J. Phys. G* **38**, 085101 (2011).
- [17] E. S. Fraga, L. F. Palhares, and P. Sorensen, *Phys. Rev. C* **84**, 011903 (2011).
- [18] L. Abreu, M. Gomes, and A. da Silva, *Phys. Lett. B* **642**, 551 (2006).
- [19] S. Yasui and A. Hosaka, *Phys. Rev. D* **74**, 054036 (2006).
- [20] L. M. Abreu, A. P. C. Malbouisson, and J. M. C. Malbouisson, *Phys. Rev. D* **83**, 025001 (2011).
- [21] M. Cristoforetti, T. Hell, B. Klein, and W. Weise, *Phys. Rev. D* **81**, 114017 (2010).
- [22] A. Bhattacharyya, P. Deb, S. K. Ghosh, R. Ray, and S. Sur, *Phys. Rev. D* **87**, 054009 (2013).
- [23] A. Bhattacharyya, R. Ray, and S. Sur, *Phys. Rev. D* **91**, 051501 (2015).
- [24] K. Fukushima, M. Ruggieri, and R. Gatto, *Phys. Rev. D* **81**, 114031 (2010).
- [25] M. N. Chernodub and A. S. Nedelin, *Phys. Rev. D* **83**, 105008 (2011).
- [26] S. Borsányi *et al.* (Wuppertal-Budapest Collaboration), *JHEP* **09**, 073 (2010).
- [27] Z.-F. Cui, F.-Y. Hou, Y.-M. Shi, Y.-L. Wang, and H.-S. Zong, *Ann. Phys.* **358**, 172 (2015).
- [28] Y. Hatta and T. Ikeda, *Phys. Rev. D* **67**, 014028 (2003).
- [29] P. Costa, M. C. Ruivo, and C. A. de Sousa, *Phys. Rev. D* **77**, 096001 (2008).
- [30] Y. Lu, Y.-L. Du, Z.-F. Cui, and H.-S. Zong, *Eur. Phys. J. C* **75**, 495 (2015).
- [31] B. Svetitsky and L. G. Yaffe, *Nucl. Phys. B* **210**, 423 (1982).
- [32] R. D. Pisarski and F. Wilczek, *Phys. Rev. D* **29**, 338 (1984).
- [33] A. Bhattacharyya, R. Ray, S. Samanta, and S. Sur, *Phys. Rev. C* **91**, 041901 (2015).
- [34] R.-A. Tripolt, J. Braun, B. Klein, and B.-J. Schaefer, *Phys. Rev. D* **90**, 054012 (2014).
- [35] S.-S. Xu, Z.-F. Cui, B. Wang, Y.-M. Shi, Y.-C. Yang, and H.-S. Zong, *Phys. Rev. D* **91**, 056003 (2015).
- [36] V. V. Braguta, E.-M. Ilgenfritz, A. Y. Kotov, B. Petersson, and S. A. Skinderev, *Phys. Rev. D* **93**, 034509 (2016).
- [37] J. Chao, P. Chu, and M. Huang, *Phys. Rev. D* **88**, 054009 (2013).
- [38] P. V. Buividovich, *Phys. Rev. D* **90**, 125025 (2014).
- [39] M. Habich, J. L. Nagle, and P. Romatschke, *Eur. Phys. J. C* **75**, 1 (2015).
- [40] Y. Hirono and E. Shuryak, *Phys. Rev. C* **91**, 054915 (2015).
- [41] P. Bożek and W. Broniowski, *Phys. Lett. B* **720**, 250 (2013).
- [42] A. Bzdak, B. Schenke, P. Tribedy, and R. Venugopalan, *Phys. Rev. C* **87**, 064906 (2013).
- [43] G. Gräf, M. Bleicher, and Q. Li, *Phys. Rev. C* **85**, 044901 (2012).